ADVANCED FUNCTIONAL MATERIALS
www.afm-journal.de

www.MaterialsViews.com

Tailored Hydrogel Membranes for Efficient Protein Crystallization

Gianluca Di Profio, Mariella Polino, Fiore P. Nicoletta, Benny D. Belviso, Rocco Caliandro, Enrica Fontananova, Giovanni De Filpo, Efrem Curcio, and Enrico Drioli*

Crystallization still represents the bottleneck in the process of protein structure determination at high resolution, despite high-throughput structural genomics programs requiring optimized crystallization strategies regarding crystal quality, time, success rate, reproducibility, and used protein amount. On the other hand, the development of suitable materials for controlled heterogeneous nucleation might facilitate biomacromolecular crystallization in a variety of experimental conditions which are not conventionally fruitful. Here, the possibility to fabricate hydrogel membranes displaying controlled chemical composition and nanostructure and to use them as heterogeneous supports for biomacromolecular crystallization is demonstrated. Diverse gel morphologies are obtained by controlling phase separation kinetics during gel layer formation on membrane support. These composite materials are found to increase the efficiency of the crystallization process so that crystals with enhanced diffraction properties are produced at lower protein concentration than conventional technique, thus affording the possibility to improve current approaches to protein crystallization and to be adapted to specific targets.

1. Introduction

Recent advances in functional genomics research have provided new gene sequence data of biological systems. Combining these information with 3D structure-function correlations on the proteins this sequences encode affords elucidation on the basic biochemical mechanisms occurring in living bodies, which are essential to develop mired therapies.[1] However, determination of proteins 3D structures by X-ray diffraction requires high quality crystals for accurate structural details.[2] Nevertheless, protein crystallization from solution presents added complexities stemming from relatively weak intermolecular interactions, flexible molecular conformations, contribution of solvent on molecular aggregation, and intrinsic evolutionary development towards the avoidance of spontaneous aggregation in the living cell environment.[3] On the other hand, the development of suitable materials for controlled heterogeneous nucleation might facilitate biomacromolecular crystallization in a variety of experimental conditions which are not conventionally fruitful.[4–6] Therefore, a multiplicity of substrates, able to force molecules to come together by chemical[7,8] or physical constrains,[9–12] were investigated so far with the objective to obtain diffraction-quality crystals.

In contrast to rigid porous materials, cross-linked soft polymer microparticles or microgels are unique in their ability to concentrate solute molecules via thermodynamic partitioning driven by favorable polymer-solute interactions. The use of viscous gels as growing media generally affords to obtain protein crystals with greater sizes, fewer defects and enhanced diffraction properties than crystals grown in solution, because of the suppression of convection currents, sedimentation, and reduced random collisions between molecules.[13] Despite that, the main problem related to the use of gels as growing media for protein crystals is the requirement to be properly supported to make them handily. Also, the conventional ways to delivery proteins and precipitants inside the gel network, to create supersaturation, and crystals recovery might include several and uneasy procedures.[14]

On these basis, the fundamental idea of this study is to improve current approaches to protein crystallization by developing functional structured materials (composite or hydrogel membranes) useful to combine the general advantages of crystallization in gel (reproducibility, size increase, and mechanical stability of crystals) with those of membrane-assisted

Dr. G. Di Profio, Dr. E. Fontananova
National Research Council of Italy (CNR)
Institute on Membrane Technology (ITM)
Via P. Bucci c/o Università della Calabria Cubo 17/C, 87036 Rende (CS), Italy
E-mail: g.diprofio@itm.cnr.it
Dr. M. Polino
University of Calabria
Department of Pharmacy
Health and Nutritional Sciences
Via P. Bucci, Ed., Polifunzionale, 87036 Rende (CS), Italy
Prof. F. P. Nicoletta, Prof. G. De Filpo
University of Calabria
Department of Chemistry and Chemical Technologies
Via P. Bucci Cubo 15/C, 87036 Rende (CS), Italy
Dr. B. D. Belviso, Dr. R. Caliandro
National Research Council of Italy (CNR)
Institute of Crystallography (IC)
Via G. Amendola 122/o, 70125 Bari (BA), Italy
Dr. E. Curcio, Prof. E. Drioli
University of Calabria
Department of Environmental and Chemical Engineering
Via P. Bucci Cubo 15/C, 87036 Rende (CS), Italy

DOI: 10.1002/adfm.201302240

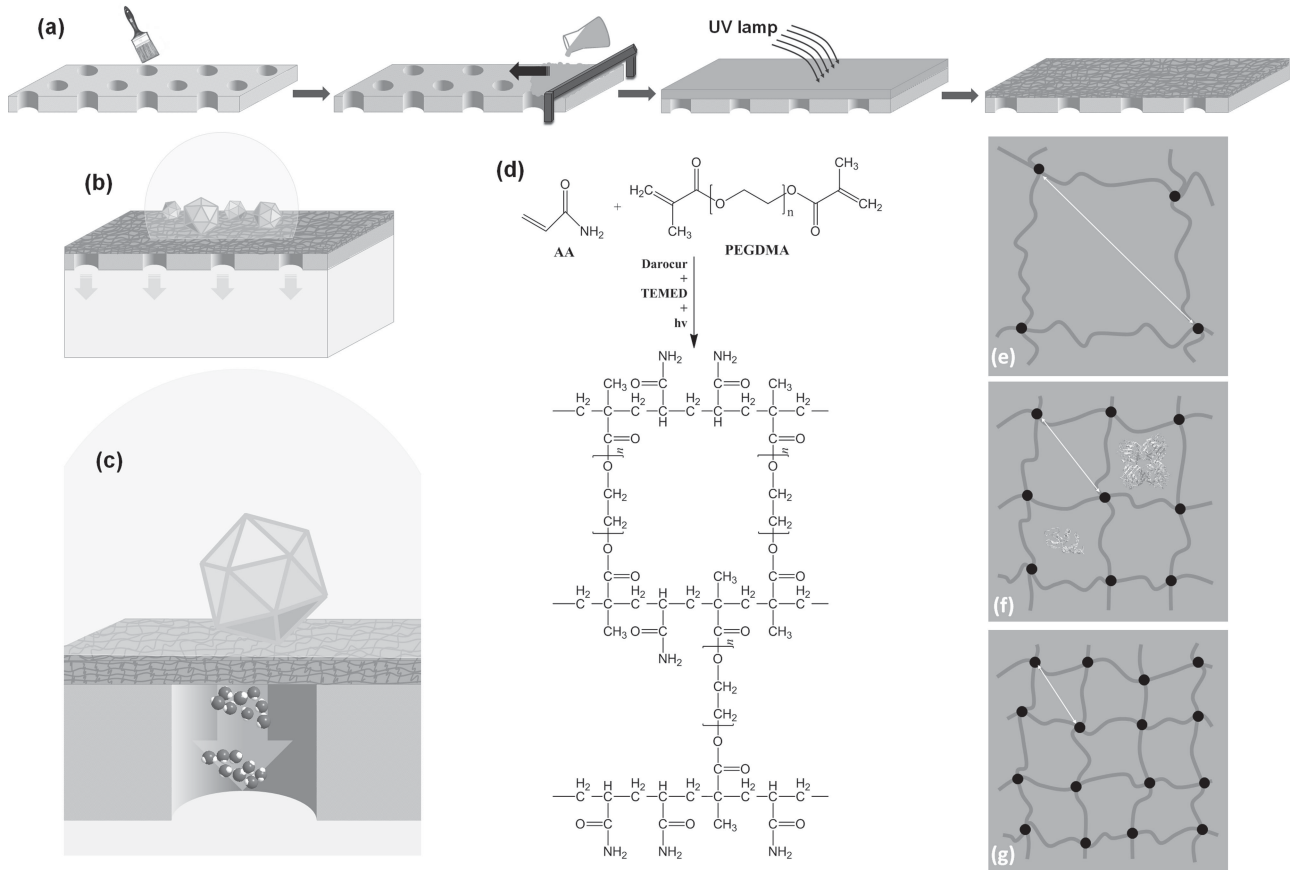

Figure 1. a) Fabrication of hydrogel membranes. b) Experimental membrane-assisted crystallization setup: a droplet of the macromolecular solution sits above the composite membrane; the membrane provides the physical contact with the reservoir (stripping) solution (down) so that only volatile solvent molecules migrate in vapor phase trough the dry pores of the substrate (gel and membrane), from the crystallizing towards the stripping solution, under the action of the driving force; as the protein solution concentrates inside the droplet, supersaturation allows nucleation and crystal growth. c) Magnification of the crystallization system at one idealized pore, showing the mechanism described above. d) Scheme of the polymerization reaction producing hydrogel network; the degree of crosslinking among fragments increases as the molar fraction of PEGDMA rises. e–g) Different hydrogel network mesh sizes obtained by changing the molar ratio between the monomer and the crosslinker: the mesh size reduces as the fraction of crosslinker increases in the mixture. In (f), the size of the macromolecules HEWL and CONA is compared with the calculated average mesh size of the hydrogel membrane C (ξ = 7.1 nm). Mesh size in (e,g) are purely speculative.

crystallization[15] (control of the process, extended optimization conditions, reduced crystallization time, and application to specific targets).

2. Results and Discussions

Earlier researches on membrane-supported hydrogels were mainly related to gel-filled pore membranes with the aim of enhancing mechanical stability of the gel interpenetrated within the pore structure and modulating transport of specific components in liquid separations.[16] In other few cases, surface layered hydrogel membranes were fabricated with the purpose to reduce fouling and to enhance transmembrane fluxes in filtration operations.[16] Here, acrylamide (AA) and poly(ethylene glycol)dimethacrylate (PEGDMA) were used to fabricate thin hydrogel layers, with selected properties, and supported on polypropylene (PP) membranes. Contrary to previous works, in this study gel intrusion inside the pores of the support was undesired in order to avoid high-resistance to mass transport in solvent evaporation membrane crystallization.[15] Accordingly, hydrogel membranes were fabricated in three main steps (**Figure 1**a): 1) conditioning of PP supports to swell the polymer and to enhance its chemical affinity with the aqueous pre-polymerization solution; 2) casting of a homogeneous layer of the pre-polymerization solution above the conditioned membrane, preventing solution intrusion inside the pores; 3) rapid polymerization of the solution under the UV lamp with the formation of the gel layer (**Figure 2**a,b, upper part). By this procedure, hydrogel membranes comprising a hydrophilic thin gel layer (contact angle θ < 90°, **Table 1**) on a macroporous hydrophobic support (θ = 143°) were successfully obtained. When using hydrophilic materials as support, for example, polyethersulfone (θ = 28°), the casting solution penetrates inside the pores despite the conditioning step, thus preventing the hydrogel layer to spread uniformly above its surface. Therefore, only hydrophobic PP support membranes were used in this work.

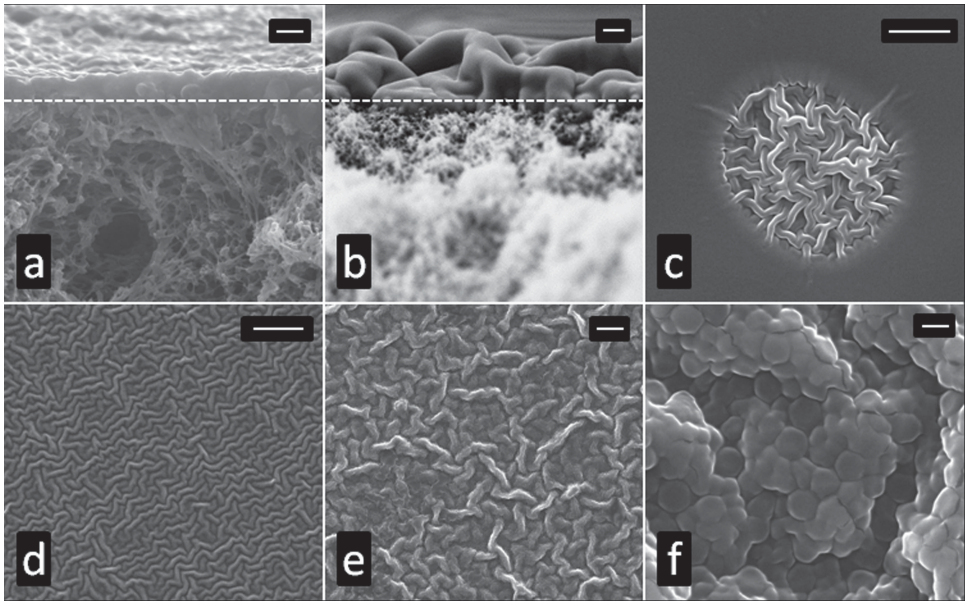

Figure 2. SEM images of hydrogel network growing on PP membranes. (a, lower part) cross section of virgin PP membrane; a) top: cross section of a dense gel layer from polymerization of a thin film (180 μm) of pre-polymer solution; b) top: bicontinuous phase morphology from polymerization of a thick film (450 μm) of pre-polymer solution. Top surface of samples showing: c) a bicontinuous phase morphology emerging from a defect in the dense skin layer; d) an open net of interconnected smooth wrinkles; e) a bicontinuous phase morphology with a sub-structure of connected-globules; and f) a zoom in the sub-structure of connected-globules. Unit bars: a) 1 μm, b) 5 μm, c) 5 μm, d) 30 μm, e) 10 μm, f) 1 μm.

Hydrogel membranes were used to contact the crystallizing and the reservoir solutions, as illustrated in Figure 1b. It is required that, under operations at atmospheric pressure, the hydrophobic membrane prevents the pores to be flooded by the two solutions so that no liquid phase mass transfer through the membrane or mixing between the two solutions occurs. Meanwhile, double liquid/vapor equilibrium establishes at mouth of each dry pore on both membrane sides. The presence of the reservoir solution provides the driving force for solvent evaporation, allowing the shift of the equilibrium with the continuous migration of water, in vapor phase, from the crystallizing towards the reservoir solution side, whereby it recondenses. As such, achieving supersaturation in the macromolecular solution allows nucleation and crystal growth, without any transfer of non-volatile components between the crystallizing and the reservoir solutions (Figure 1c).[15] This mechanism keeps working despite the presence of the hydrophilic gel layer in hydrogel membranes provided that at least one hydrophobic stratum (as that supplied by PP) separates the crystallizing and the reservoir solutions.

Table 1. Hydrogel membrane properties: monomer/crosslinker (AA/PEGDMA) molar ratio, overall solution concentration (C_p), average molecular weight between crosslinks ($\overline{M}_c$), calculated average mesh size (ξ), swelling degree (S_w), and equilibrium water contact angle (θ). Contact angle is reported also for virgin PP support

Membrane	AA/PEGDMA	C_p [wt%]	$\overline{M}_c$ [g mol^{-1}]	ξ [nm]	S_w [%]	θ [°]
A	19.0:1	6.9	10 800	16.4	25.73	54.1
B	12.3:1	7.9	5100	8.8	15.08	68.8
C	9.0:1	8.9	4200	7.1	13.21	78.2
D	7.0:1	9.9	3000	5.3	10.79	80.9
E	5.7:1	10.8	1900	3.7	8.45	82.6
F	4.7:1	11.8	1600	3.1	7.67	83.4
PP						143.1

The structure of hydrogels is typically described by the mesh size, which is related to the average molecular weight between crosslinks within the polymer network (Figure 1d).[17] The compartmentalization of the macromolecular solution within the 3D porous gel network restricts the mobility of adsorbed molecules, as such providing a confined environment for crystallization to take place (Figure 1e–g).[18] Accordingly, several hydrogel membranes (labeled as A–F in Table 1) were prepared by modifying the molar ratio between monomer (AA) and crosslinker (PEGDMA) to investigate the effect of the gel composition and nanostructure on protein crystallization. Decreasing the AA:PEGDMA molar ratio, the degree of crosslinking increases while the degree of swelling decreases (Table 1). In the same order, the density of polar terminal amidic groups ($-CONH_2$) drops, while the concentration of apolar moieties ($-OCH_2CH_2-$) rises. The change in the chemical gel layer composition is reflected by the decreasing surface polarity going from the sample A to F as water contact angle θ moves from 54° to 83°.

SEM analysis reveals that hydrogel binds to macro-porous virgin PP support (Figure 2a, lower part) giving rise to diverse morphologies which depend on the initial thickness, the overall composition of the casting solution, and the UV power. When crosslinking thinner solutions (180 μm), irrespectively of their composition, a dense layer forms on the top of PP support

Table 2. Results from the crystallization tests on HEWL and CONA with hydrogel membranes, original membranes (PP), and conventional hanging drop solvent evaporation (Reference). Numbers at the head of each protein column indicate the starting concentration of proteins (as mg mL^{-1}) in the crystallizing droplet. Precipitants were NaCl 3.5 wt% for HEWL and $(NH_4)_2SO_4$ 1.5 m for CONA at the beginning of the test (C: crystals; AP: amorphous precipitate; N: clear solution; S: spherulites). Results refer to 48 h for HEWL and to 1 week for CONA after experiments setting up, respectively.

Membrane	HEWL					CONA			
	15	20	25	30	30[a)]	2.5[b)]	7.5	10	15
PP	N	N	C	AP	S	N	N	N	C
A	C	C	C	C	C	N	N	C	C
B	C	C	C	C	C	N	N	C	C
C	C	C	C	C	C	C	N	C	C
D	C	C	C	C	C	C	C	C	C
E	N	C	C	C	C	C	C	C	C
F	N	C	C	C	C	C	C	C	C
Reference	N	N	C	AP	N	N	N	N	C

[a)]Without precipitant; [b)] Results for CONA at 2.5 mg mL^{-1} refer to 1 month from experiments setting up.

(Figure 2a, upper part). The final gel layer is thinner than the casting solution film because of water loss and gel shrinking during both polymerization and SEM sample preparation. For thicker casting solutions (450 μm), the gel layer evolves into some singular hierarchical morphologies as the AA:PEGDMA molar ratio decreases (Figure 2b): a bicontinuous phase morphology below a dense skin (Figure 2c), a net of interconnected smooth wrinkles (Figure 2d), and an open (without skin) bicontinuous morphology (Figure 2e) with a sub-structure of connected-globules (Figure 2f) is found as progressive evolution of the dense layer. The origin of these structures is due to a spinodal decomposition occurring during the photo-crosslinking reaction associated to solvent evaporation.[19] At the air-solution interface a concentrated precursors layer is formed because of solvent evaporation (also exacerbated by the thermal gradient generated by the UV irradiation). During UV irradiation this layer evolves in a crosslinked skin gel layer in the case of thinner films and thicker layers with a high AA:PEGDMA molar ratio. The solution capped by the skin layer undergoes a spinodal decomposition, which displays the typical bicontinuous phase morphologies.[20] In the case of low AA:PEGDMA molar ratios, the skin layer is very thin or does not form at all, and open sub-structured bicontinuous phase morphologies appear.

Equilibrium swelling measurements were performed to estimate the average molecular weight between crosslinks, $\overline{M_c}$, and the average mesh size, ξ. Table 1 shows that both $\overline{M_c}$ and ξ decrease with decreasing the AA:PEGDMA molar ratio.

To study the effect of the gel sub-microstructure in crystallization, thin-layer A–F hydrogel membranes were used in the experiments on the model proteins lysozyme (HEWL) and concanavalin A (CONA), and compared with conventional vapor diffusion system (reference). **Table 2** reports the macromolecular solution compositions tested and the corresponding crystallization results. Experiments with HEWL at 20–30 mg mL^{-1} resulted in the formation of faceted crystals in 48 h for all hydrogel membranes; an amorphous precipitate was obtained in the reference (conventional hanging drop vapor diffusion) and bare PP membranes at 30 mg mL^{-1}, while no crystal appeared with virgin PP and reference at 20 mg mL^{-1}. At low protein concentration (15 mg mL^{-1}), crystals formed only with A–D hydrogel membranes. Large HEWL crystals were also obtained at 30 mg mL^{-1} without precipitant for all hydrogel membranes (**Figure 3**), which preserved their properties for weeks. No crystals were obtained with conventional vapor diffusion without using precipitant (image not shown). Similar results were observed in all the 5 replicas in the wells of the crystallization plates incubated at the same conditions. Tests with CONA confirmed that the use of hydrogel membranes allows obtaining crystals at lower protein concentrations (10 and 7.5 mg mL^{-1}) with respect to reference. Here, a strong time- and size-dependence was observed: crystals of ≈200 μm grew in 48 h on hydrogel membranes, while crystals of ≈100 μm grew in 120 h in reference. Table 2 gives a snapshot after one week from the crystallization setting up, when diffraction data were taken. After one month from setting up it was noticed that: i) crystals

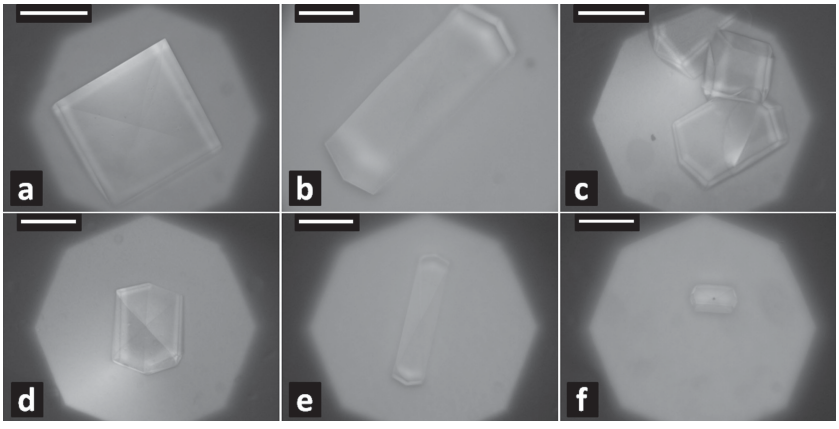

Figure 3. Optical microscopy images of HEWL crystals obtained at the protein concentration of 30 mg mL^{-1} without using precipitant: a) mesh A, b) mesh B, c) mesh C, d) mesh D, e) mesh E, f) mesh F. Unit bars: a,c) 500 μm; b–f) 200 μm.

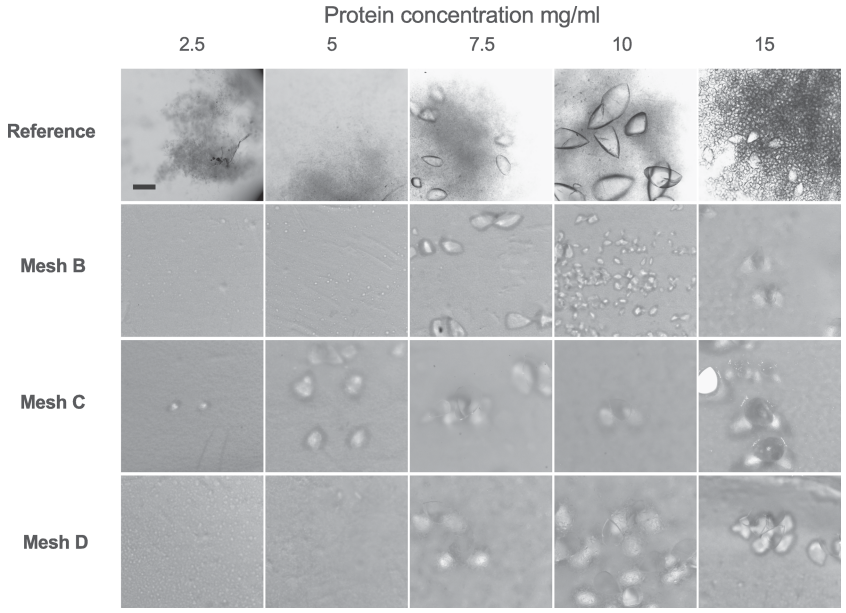

Figure 4. Optical microscopy images of some selected CONA crystals obtained at different initial protein concentrations (top) and crystallization supports (left), taken one month after the crystallization setting-up. Light transmission and reflection observation modes were used for reference and hydrogel membrane conditions, respectively.

grew also at protein concentrations lower than 7.5 mg mL^{-1} for hydrogel membranes; ii) sample C produced crystals of largest size for a wide protein concentration range (2.5 to 15 mg mL^{-1}); iii) reference produced large-sized crystals only at 10 mg mL^{-1}, amorphous precipitate at lower concentrations and a bed of small crystals at higher concentration. Selected crystal samples obtained with membrane B-D and in reference are shown in **Figure 4**. These results indicate that hydrogel membranes widen crystallization intervals by self-adjusting nucleation and growth conditions in the course of the same experiment; crystal size and grow-time are also optimized.

Analysis of diffraction quality revealed that the number of spots with good signal-to-noise ratio and the crystal mosaicity, indicating the crystal long-range disorder, increase in hydrogel membranes with respect to reference crystals (**Figure 5**a,b), while no definite trend was found for unit cell constants (variations below 1%). For CONA, the number of spots is higher for samples C and D, where the largest crystals were obtained (cf. Figure 4). Results from the full crystal structure determination, carried out on representative crystals for the two proteins, confirmed these findings (**Table 3**) and allowed comparing the obtained structural models (Figure 5c). It was found that the calculated moduli (R, R_{free}) and phases (MPE) are better for hydrogel membrane crystals than for reference ones, consistently in all resolution shells. Overall crystallographic results can be interpreted by considering that protein crystal lattice is able to incorporate large amounts of gels.[21] This leads to an increase both in crystal size, with a consequent increase of the spot intensities, and in crystal mosaicity, related to larger spot sizes. Our findings prove that by using hydrogel membranes the latter effect is minority with respect to the former, which lead to improved spot statistics, hence to more accurate structural models. The low variations of lattice constants point out that no inclusion of contaminants coming from gel or membrane has taken place, since this usually lead to lattice distortions for impurities having molecular dimensions comparable to that of the hosting molecule.[22] In addition, the structural resolution performed on two crystals grown on hydrogel did not revealed electron densities attributable to foreign molecules.

Crystallization results demonstrated the auto-regulation of the gel in adjusting the optimal amount of solute molecules, concentrating them in the porous network[23] till to the production of diffraction-quality crystals. Equilibrium adsorption isotherms reported in **Figure 6** for both HEWL and CONA, display a bimodal profile, suggesting that two different adsorption modes, operating at low and higher protein concentration, occur.[24] Langmuir-Freundlich model, which takes both heterogeneous adsorption sites and interactions among the adsorbed molecules into account, provides the best fitting to data points. Fitting procedure gave heterogeneity index n (describing the cooperation degree in the adsorption) in the range 0.35–0.98 for low concentrations, indicating non-cooperative random adsorption, and in the range 8.64–2.45 for high solute concentrations, meaning attractive interactions. The transition from non-cooperative to cooperative adsorption occurs around to a threshold concentration (≈27 mg mL^{-1} for HEWL and ≈4.5 mg mL^{-1} for CONA), which is independent on the mesh size, and discriminates whether crystals form. Note that protein and precipitant solution concentrations reported in Table 2 are initial values at the moment that the macromolecular and the reservoir solutions droplets are mixed together. As the crystallization test proceeds under the action of driving force, the overall crystallizing solution concentrates because of solvent (water) evaporation, so that the final concentration just before the crystallization takes place is almost doubled (somewhat less) with respect to its starting value. Accordingly, with hydrogel membranes, crystals were obtained at the threshold protein concentration of ≈30 mg mL^{-1} for HEWL (after 48 h) and ≈5 mg mL^{-1} for CONA (after one month), respectively.

This implies that proteins adsorption is not affected by the different nanostructure of the gel (mesh size), but instead it depends on the chemical affinity between the gel network and proteins, modulated by the chemical composition of the gel layer. Hydrophobic regions in the gel network increase as the cross-linker density rises (θ and $1/\overline{M_c}$ in Table 1). HEWL, with isoelectric point (pI) 10.6, is positively charged at *p*H 4.6, while CONA, having pI 4.5–5.5, has null net charge at pH 4.9. Accordingly, HEWL displays increasing affinity for network with higher density of polar groups (higher amount of AA amidic groups), while CONA better interacts when the apolar moieties in the gel net increase (higher crosslinker density). This result confirms the higher tendency for HEWL to nucleate with polar substrates while CONA shows a preferred affinity for apolar substrates,[25] and highlight the fundamental role of the chemical nature

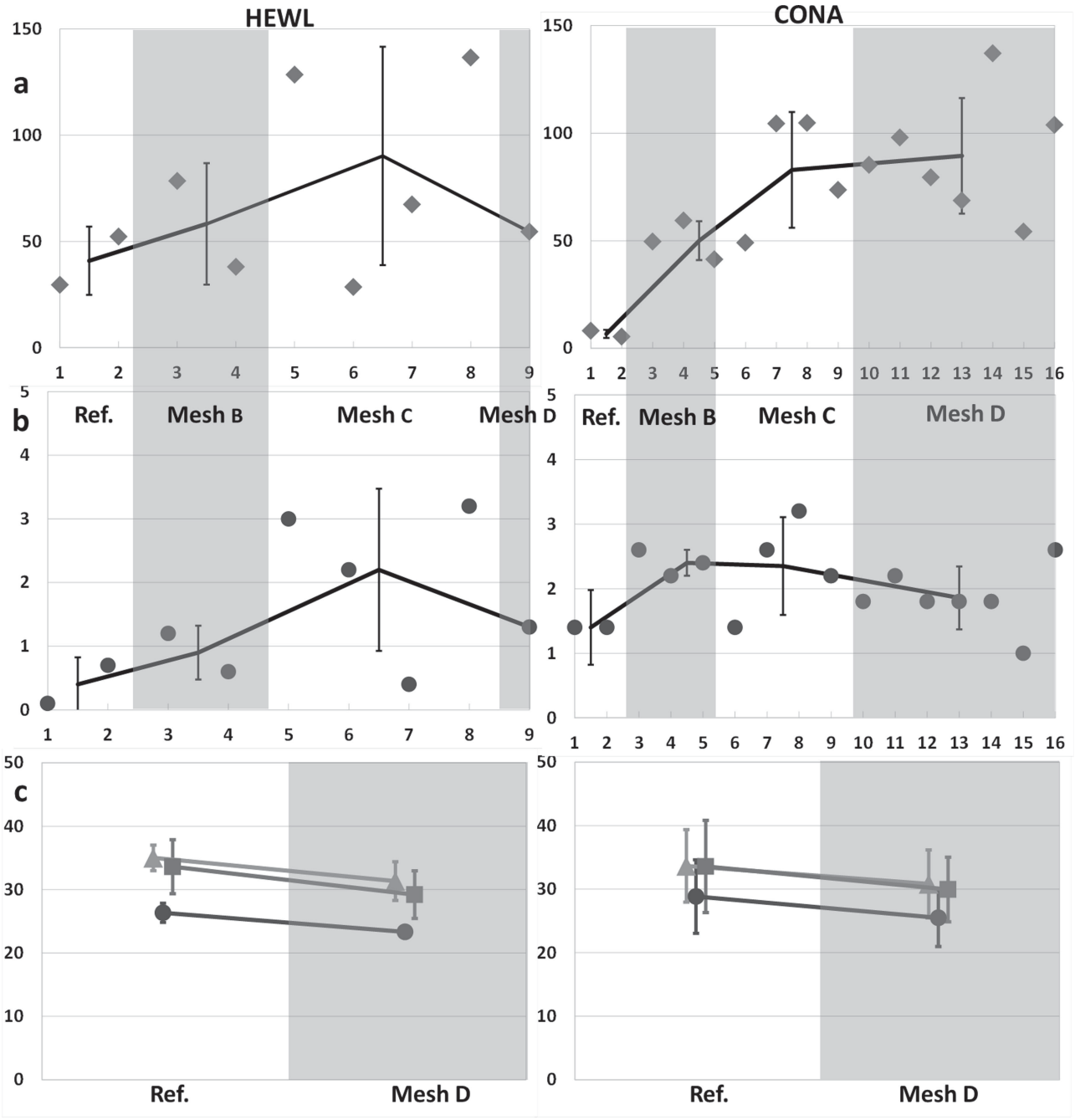

Figure 5. a) Number of spots per image with $I/\sigma > 20$ and b) mosaicity for the crystals analyzed by short scans of HEWL (left) and CONA (right). Mean values and their standard deviations are connected by a line. c) Parameter assessing the quality of the structural models, obtained from selected crystal analyzed by long scans: biased agreement factor of calculated versus observed moduli R (circles), unbiased agreement factor R_{free} (triangles), and mean phase error (squares). Error bars indicate the standard deviations of the parameter values calculated in each resolution shell. Vertical shaded areas separate the crystallization conditions.

of templates in influencing the crystallization kinetics.[25,26] Accordingly, selecting hydrogel membranes with a specific chemical composition allows direct influence on crystallization. In the specific case of hydrogel membranes investigated in this study, the chemical character of the network prevails over the gel nanostructure in addressing the crystallization pathway, so that confinement effects were not observed at this stage.

3. Conclusions

In summary, we demonstrated the possibility to fabricate composite polymeric membranes supporting a homogeneous thin hydrogel layer, displaying tailored chemical composition, nano-architecture (mesh size) and selected morphologies. The proposed approach provides suitable tools for efficient protein

Table 3. Crystallographic data for hydrogel membranes with mesh-D gel and reference crystals

	CONA		HEWL	
	Reference	PP/D	Reference	PP/D
Space group	I 2 2 2	I 2 2 2	P 43 21 2	P 43 21 2
Unit cell parameters [Å]				
a	61.72	61.90	78.73	77.97
b	86.97	86.33	78.73	77.97
c	89.31	88.77	37.11	37.42
Resolution range [Å]	62.31–1.94	61.89–1.94	55.671–1.94	55.671–1.94
(outer shell)	(2.04–1.94)	(2.05–1.94)	(2.05–1.94)	(2.05–1.94)
Unique reflections	16462	16382	8349	8210
Redundancy	6.5	6.0	11.7	11.1
$<I/\mathrm{sig}(I)>$	4.8	10.1	33.5	19.0
Completeness [%]	90.8	91.1	91.6	91.2
R_{merge} [%]	0.26	0.11	0.05	0.09
Mosaicity [°]	0.05	1.49	0.61	1.18
Total rotation angle [°]	180	180	90	90
B [Å^2]	18.4	15.9	10.1	17.2

crystallization, affording a crystallization platform in which protein and additives are easily delivered to the gel network, where supersaturation is generated by gradual solvent removal in vapor phase through the porous structure of both support membrane and hydrogel layer, and crystals are easily recovered. The method was found to increase the efficiency of the crystallization process so that crystals appeared at lower protein concentration and demonstrated enhanced diffraction features. As perspective, the method can be optimized to create an environment compatible with membrane proteins crystallization, as platform for biomineralization and polymorphs selection studies, and can provide routes to access non-classical mesocrystal structures.

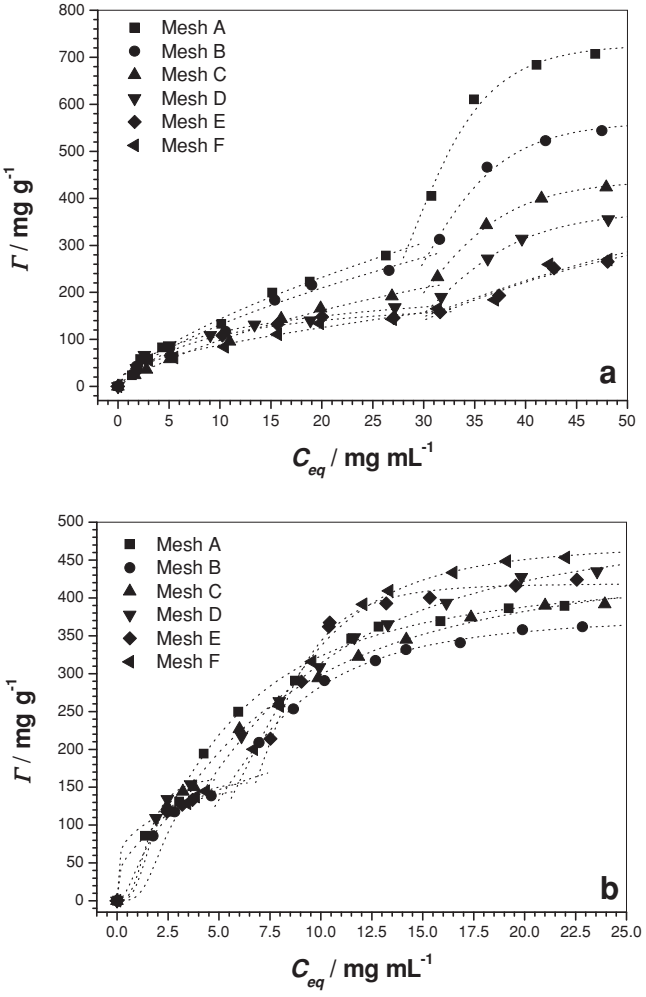

Figure 6. Adsorption isotherms for a) HEWL and b) CONA on hydrogel membranes with different mesh size (A–F). Dotted curves are the best fittings of experimental data by Langmuir-Freundlich equation. Γ is the amount of solute adsorbed per weight of adsorbent (hydrogel); C_{eq} is the equilibrium concentration of solute.

4. Experimental Section

Materials: The monomer acrylamide (cod. 01700, from Fluka), the crosslinker poly(ethylene glycol)dimethacrylate (average molecular weight 750 Da, cod. 437468, from Sigma-Aldrich), the catalyst N,N,N′,N′-tetramethylethylenediamine (TEMED, cod. 411019, from Sigma-Aldrich), and the photoinitiator Darocur 1173 (2-hydroxy-2methyl-1-phenyl-propan-1-one, with a maximum absorption at around 250 nm, cod. 1830961, from Ciba) were used as received. The pre-polymer solutions were prepared by dissolving AA and PEGDMA, in the molar ratio 19.0:1 (A), 12.3:1 (B), 9.0:1 (C), 7.0:1 (D), 5.7:1 (E), and 4.7:1 (F), in a water solution containing the photoinitiator (0.6 vol%) and TEMED (1.5×10^{-3} vol%).

Chicken hen egg white lysozyme (cod. 62970, from Sigma-Aldrich) was dissolved in sodium acetate buffer (0.1 m, pH 4.6) at the initial concentration 10, 20, 30, 40, 50, 60 mg mL^{-1}. Sodium Chloride (NaCl, 7.0 wt%, cod. 131659.1211, from Panreac), dissolved in the same buffer, was used as precipitant agent for HEWL. Concanavalin A from Canavalia Ensiformis (cod. C7275, from Sigma-Aldrich) was dissolved in sodium citrate buffer (0.1 m, pH 4.9) at the concentration of 5, 10, 15, 20, 30 mg mL^{-1}. The precipitant solution for CONA was composed by $(NH_4)_2SO_4$ (1.5 m, cod. 204501, from Sigma-Aldrich) in the same buffer. All protein solutions were prepared by using HPLC grade water (cod. 23595.328, from VWR) and filtered by 0.45 µm nominal pore size PTFE filter (cod. SLLHR04NL, Millex-LH) before use.

Hydrogel Membranes Preparation: Hydrogel membranes were prepared by the following steps: 1) Commercial polypropylene (Accurel PP2EHF) and polyethersulfone membranes (PES, MicroPes 2F from Membrana GmbH) were pre-treated by soaking with methanol (CH_3OH, HPLC grade, cod. 20844.320, from VWR) for 24 h at room temperature; 2) the pre-polymer solution was cast onto the membrane by a micrometric film applicator with adjustable thickness (Elcometer 3570) or by rolling on the loaded support with a bar coater at 180 and 450 µm; 3) crosslinking polymerization of solution was achieved by a high pressure mercury lamp (Philips HPK 125, 500 mW cm^{-2} @ 253 nm, irradiation time 5 min) which provided the formation of the gel layer above the support membrane surface (Figure 1a). Before use in crystallization tests, hydrogel membranes were extensively washed with bi-distilled water, to remove methanol and residual traces of unreacted AA and PEGDMA, dried, and stored at 30 °C until no significant variation in weight was detected over three successive checks.

Hydrogel Membranes Characterizations: Equilibrium water contact angles (θ) were measured using CAM 200 contact angle meter (KSV

Instruments Ltd.) equipped with microsyringe, automatic dispenser, and software for image acquisition and processing. Contact angles were calculated as the average of three different measurements for each one of three slices of the same membrane surface.

Morphological analysis was performed by a Quanta 200F FEI Philips scanning electron microscope (SEM). Membranes were placed on appropriate stubs and then sputtered with chromium or gold under an argon atmosphere (in an Emitech K575X Peltier) to achieve the necessary conductivity. To analyze membrane section, membranes were cryo-fractured with liquid nitrogen. The accelerating voltage was 12.5 kV under high vacuum conditions.

In order to investigate the changes in the hydrogel microstructure, equilibrium swelling measurements were performed to estimate the average molecular weight between crosslinks, $\overline{M}_c$, and the average mesh size, ξ, of hydrogel layers. The mesh size was calculated by the Flory-Rehner theory for hydrogels prepared in the presence of water modified by Peppas & Merril,[27,28] and using literature values of model parameters.[29,30] In particular, $\overline{M}_c$, was calculated by the following equation:

$$\frac{1}{\overline{M}_c} = \frac{2}{\overline{M}_n} - \frac{\bar{v}/V_1\left[\ln\left(1-v_{2,s}\right)+v_{2,s}+\chi_1 v_{2,s}^2\right]}{v_{2<r}\left[\left(\frac{v_{2,s}}{v_{2,r}}\right)^{1)3}-\left(\frac{v_{2,s}}{2v_{2,r}}\right)\right]} \quad (1)$$

where $\bar{v}$ is the specific volume of poly-AA (0.768 cm^3 g^{-1}), V_1 the solvent molar volume (water, 18 cm^3 mol^{-1}), χ_1 the polymer-solvent interaction parameter (0.494 for poly-AA and water), $v_{2,s}$ and $v_{2,r}$ the polymer volume fraction in the swollen and relaxed states, respectively. $\overline{M}_n$ is the molecular weight of the polymer chains prepared in the absence of crosslinking agent, and was estimated from the measurement of polymer intrinsic viscosity, [η], at 25 °C by an Ubbelohde capillary viscosimeter and using the following relation of Klein and Conrad:[31]

$$[\eta] = 4.9 \times 10^{-3}\,\overline{M}_n{}^{0.80} \quad (2)$$

Finally, the mesh size was calculated by:[27]

$$\xi = v_{2,s}^{-1/3}\left(\frac{2C_n\overline{Mc}}{Mr}\right)^{1/2} l \quad (3)$$

where C_n is the Flory characteristic ratio (6.32), l the length of the bond along the polymer backbone (1.54 Å), M_r the molecular weight of the repeating units from which the polymer chain is formed.

Protein Adsorption Isotherms on Hydrogel Membranes: Adsorption isotherms were obtained by batch method. Weighted 1 cm wide disks of each hydrogel membrane (mesh size A–F) were immersed in 500 µL protein solutions at given initial concentrations, ranging from 0.5 to 50 mg mL^{-1} for HEWL and from 0.5 to 20 mg mL^{-1} for CONA, in the same buffer used for crystallization tests, and left to equilibrate for 24 h at 20 ± 0.1 °C in a thermostatic box. After that, the absorbance of the supernatant at 280 nm was determined by an UV spectrophotometer (Shimadzu UV-1601), while hydrogel membranes were weighted again. The amount of protein adsorbed per unit mass of adsorbent was determined by mass balance.

Protein Crystallization: For each protein, 5 µL drop solutions were pipetted on the surface of the hydrogel membrane and added with the equal volume of precipitant solution. For each tested condition, 5 replica experiments were carried out by introducing samples in the array of wells of screw top hanging drop plates (EasyXtal 15-well Tool, Qiagen) where 500 µL of precipitant solutions were used as reservoir (or stripping) agents. Plates were then incubated at 20 ± 0.1 °C before optical microscopy inspection of the droplets after 48 h for HEWL and 1 week for CONA, and then stored at 20 ± 0.1 °C for successive observations. Experiments were also performed as described above using virgin PP membranes and by conventional hanging drop vapor diffusion method (reference).

Crystals' Characterization: Protein crystals were observed under an optical microscope (DM 2500M, Leica Microsystems) equipped with a videocamera.

Crystals from hydrogel membranes and reference experiments were handled in the same way. They were transported together in the plates from the crystallization to the diffractometer sites. Here they were mounted using cryo-loops, without using any cryo-protectant, so that gel surrounded the crystals during the measurements. Diffraction data were collected at diffractometer RIGAKU, equipped by a CuKα rotating anode and a SATURN 944 CCD detector. The oscillation frame was set to 0.5°, the exposure time to 5 s, and the detector distance was set at the minimum allowed to take high-resolution data. Data were taken in cryogenic conditions, following two strategies: short (36 images) and long (360 images) scan of the asymmetric unit. The first was applied on a number of crystals (9 for HEWL, 16 for CONA) for monitoring their diffraction properties, the second on selected crystals (one from hydrogel membrane and one from reference for each protein) for assessing the results of the phasing process. Diffraction data were indexed by MOSFLM;[32] long scan data were reduced by POINTLESS and SCALA,[33] and phased by the molecular replacement (MR) program REMO[34] of the package IL MILIONE,[35] with structural models 1LYS and 3CNA for HEWL and CONA, respectively. MR solutions were refined without manual intervention by using ARP-WARP[36] and REFMAC[37] packages, and final models were validated by using the program MOLPROBITY.[38]

Acknowledgements

Authors are grateful to Giuseppe Chita (from CNR-IC, Bari) for his help in crystal production and monitoring, and to Giosuè Sorrentino (from CNR-IBB, Napoli) for his support in X-ray measurements. Authors also thank Dr. Mariano Davoli (from University of Calabria, Rende) for providing SEM analysis support.

Received: July 2, 2013
Revised: September 2, 2013
Published online: October 22, 2013

[1] B. G. Fox, C. Goulding, M. G. Malkowski, L. Stewart, A. Deacon, *Nat. Methods* **2008**, *5*, 129–132.
[2] A. McPherson, *Crystallization of biological macromolecules* Cold Spring Harbor Laboratory Press, New York, **1999**.
[3] J. P. K. Doye, A. A. Louis, M. Vendruscolo, *Phys. Biol.* **2004**, *1*, 9–13.
[4] N. E. Chayen, E. Saridakis, *Nat. Methods* **2008**, *5*, 147–153.
[5] A. S. Myerson, *Handbook of industrial crystallization* 2nd ed., Butterworth-Heinemann, Woburn, MA, **2002**.
[6] N. E. Chayen, E. Saridakis, *Trends Biotechnol.* **2008**, *27*, 99–106.
[7] G. Falini, S. Fermani, G. Conforti, A. Ripamonti, *Acta Crystallogr. D* **2002**, *58*, 1649–1652.
[8] T. Pham, D. Lai, D. Ji, W. Tuntiwechapikul, J. M. Friedman, T. R. Lee, *Colloids Surf. B* **2004**, *34*, 191–196.
[9] N. E. Chayen, E. Saridakis, R. El-Bahar, Y. Nemirovsky, *J. Mol. Biol.* **2001**, *312*, 591–595.
[10] E. Curcio, E. Fontananova, G. Di Profio, E. Drioli, *J. Phys. Chem. B* **2006**, *110*, 12438–12445.
[11] U. V. Shah, D. R. Williams, J. Y. Y. Heng, *Cryst. Growth Des.* **2012**, *12*, 1362–1369.
[12] A. McPherson, P. Shlichta, *Science* **1988**, *239*, 385–387.
[13] J. M. García-Ruiz, M. L. Novella, R. Moreno, J. A. Gavira, *J. Cryst. Growth* **2001**, *232*, 165–172.
[14] Y. Li, D. Guo, B. Zheng, *RSC Adv.* **2012**, *2*, 4857–4863.
[15] G. Di Profio, E. Curcio, E. Drioli *Ind. Eng. Chem. Res.* **2010**, *49*, 11878–11889.
[16] Q. Yang, N. Adrus, F. Tomicki, M. Ulbricht, *J. Mater. Chem.* **2011**, *21*, 2783–2811.

[17] T. Canal, N. A. Peppas, *J. Biomed. Mater. Res.* **1989**, *23*, 1183–1193.
[18] Y. Diao, M. E. Helgeson, A. S. Myerson, T. A. Hatton, P. S. Doyle, B. L. Trout, *J. Am. Chem. Soc.* **2011**, *133*, 3756–3759.
[19] L. Wang, Z. Zhang, Y. Ding, *Soft Matter* **2013**, *9*, 4455–4463.
[20] B. D. Ermi, A. Karim, J. F. Douglas, *J. Polymer Sci. B* **1998**, *36*, 191–200.
[21] J. M. García-Ruiz, J. A. Gavira, F. Otálora, A. Guash, M. Coll, *Mater. Res. Bull.* **1998**, *33*, 1593–1598.
[22] A. A. Chernov, *Phys. Rep.* **1997**, *288*, 61–75.
[23] B. Lorber, C. Sauter, A. Théobald-Dietrich, A. Moreno, P. Chellenberger, M.-C. Robert, B. Capelle, S. Sanglier, N. Potier, R. Giegé, *Prog. Biophys. Mol. Biol.* **2010**, *101*, 13–25.
[24] B. Al-Duri, Y. P. Yong, *Biochem. Eng. J.* **2000**, *4*, 207–215.
[25] U. V. Shah, M. C. Allenby, D. R. Williams, J. Y. Y. Heng, *Cryst. Growth Des.* **2012**, *12*, 1772–1777.
[26] G. Di Profio, E. Fontananova, E. Curcio, E. Drioli, *Cryst. Growth Des.* **2012**, *12*, 3749–3777.
[27] N. A. Peppas, E. W. Merril, *J. Appl. Polym. Sci.* **1977**, *21*, 1763–1770.
[28] N. A. Peppas, J. Z. Hilt, A. Khademhosseini, R. Langer, *Adv. Mater.* **2006**, *18*, 1345–1360.
[29] D. Saraydin, E. Karadag, Y. Isikver, N. Sahiner, O. Guven, *J. Macromol. Sci. A* **2004**, *41*, 419–431.
[30] J. Rosiak, K. Burczak, T. Czolczynska, W. Pekala, *Rad. Phys. Chem.* **1983**, *22*, 917–928.
[31] J. Klein, K. D. Conrad, *Makromol. Chem.* **1978**, *179*, 1635–1638.
[32] A. G. W. Leslie, *Acta Crystallogr. D* **2006**, *62*, 48–57.
[33] P. Evans, *Acta Crystallogr. D* **2006**, *62*, 72–82.
[34] R. Caliandro, B. Carrozzini, G. L. Cascarano, L. De Caro, C. Giacovazzo, A. Mazzone, D. Siliqi, *J. Appl. Cryst.* **2006**, *39*, 185–193.
[35] M. C. Burla, R. Caliandro, M. Camalli, B. Carrozzini, G. L. Cascarano, L. De Caro, C. Giacovazzo, G. Polidori, D. Siliqi, R. Spagna, *J. Appl. Cryst.* **2007**, *40*, 609–613.
[36] S. X. Cohen, M. B. Jelloul, F. Long, A. Vagin, P. Knipscheer, J. Lebbink, T. K. Sixma, V. S. Lamzin, G. N. Murshudov, A. Perrakis, *Acta Crystallogr. D* **2008**, *64*, 49–60.
[37] P. Skubák, G. N. Murshudov, N. S. Pannu, *Acta Crystallogr. D* **2004**, *60*, 2196–2201.
[38] V. B. Chen, W. B. Arendall, J. J. Headd, D. A. Keedy, R. M. Immormino, G. J. Kapral, L. W. Murray, J. S. Richardson, D. C. Richardson, *Acta Crystallogr. D* **2010**, *66*, 12–21.